Metallophysics and Advanced Technologies
Металофіз. новітні технол.
Metallofiz. Noveishie Tekhnol.
2022, vol. 44, No. 9, pp. 1163–1177
https://doi.org/10.15407/mfint.44.09.1163
Reprints available directly from the publisher

PACS numbers: 61.46.-w, 61.48.De, 61.72.-y, 65.80.+n, 68.35.Rh

Fabrication, Optimization, and Mechanism Analysis of Graphene/Hexagonal Boron Nitride Stacked Film

L. Zhang, X. T. Wang, N. X. Ci, R. Q. Peng, G. Q. Zhao, L. J. Ci, and G. H. Min

Key Laboratory for Liquid-Solid Structural Evolution and Processing of Materials, Ministry of Education, Shandong University, 250061 Jinan, P. R. China

Stacked structures of graphene/hexagonal boron nitride (G/h-BN) exhibit high carrier mobility, thermal stability, and deep ultraviolet absorption properties which are considered important for developing various novel devices. However, the realization of their large-scale fabrication and the improvement of performance are technically limited by the complicated exfoliation and transfer processes during fabrication. In this study, the h-BN film was successfully deposited by RF-magnetron sputtering and was used as an alternative to metal catalysts in the synthesis of graphene *via* low pressure chemical vapour deposition. This provides an alternative strategy to avoid any exfoliation and transfer processes in the development of G/h-BN stacked structures. The stacked structure was confirmed by Raman spectroscopy, atomic force microscopy, and x-ray photoelectron spectroscopy. The stacked films were found to be uniform, continuous and well doped with boron and nitrogen. The fabrication parameters were optimized to obtain high-quality graphene, and the formation mechanism of graphene on the BN film was also investigated.

Key words: hexagonal boron nitride, graphene, stacked film, RF-magnetron sputtering, chemical vapour deposition.

Багатошарові структури з графену/гексагонального нітриду бору (G/h-BN) демонструють високу рухливість носіїв, термічну стабільність і влас-

Corresponding author: Lin Zhang and Guoqing Zhao
E-mail: zhanglin2007@sdu.edu.cn, guoqingzhao@sdu.edu.cn

Citation: L. Zhang, X. T. Wang, N. X. Ci, R. Q. Peng, G. Q. Zhao, L. J. Ci, and G. H. Min, Fabrication, Optimization, and Mechanism Analysis of Graphene/Hexagonal Boron Nitride Stacked Film, *Metallofiz. Noveishie Tekhnol.*, **44**, No. 9: 1163–1177 (2022). DOI: 10.15407/mfint.44.09.1163

тивості глибокого поглинання ультрафіолетового випромінювання, які вважаються важливими для розробки різноманітних нових пристроїв. Однак їх широкомасштабне виготовлення та покращення продуктивності технічно обмежено складними процесами відшарування та перенесення під час виготовлення. У цьому дослідженні плівка h-BN була успішно нанесена за допомогою радіочастотного магнетронного розпилення та використовувалася як альтернатива металевим каталізаторам завдяки синтезу графена шляхом хемічного осадження з газової фази під низьким тиском. Це забезпечує альтернативні можливості для уникнення будь-яких процесів відшарування та перенесення при розробці багатошарових структур G/h-BN. Багатошарову структуру було підтверджено за допомогою спектроскопії комбінаційного розсіювання, атомно-силової мікроскопії та рентґенівської фотоелектронної спектроскопії. Було встановлено, що багатошарові плівки є однорідними, суцільними та добре леґованими Бором і Нітроґеном. Було оптимізовано параметри виготовлення для одержання високоякісного графену, а також досліджено механізм формування графену на плівці BN.

Ключові слова: гексаґональний нітрид бору, графен, багатошарова плівка, радіочастотне магнетронне напилення, хемічне осадження з газової фази.

(Received May 11, 2021; in final version, June 15, 2022)

1. INTRODUCTION

Two dimensional (2D) atomic films, such as graphene [1], hexagonal boron nitride (h-BN) [2], and MoS_2 [3], have been discovered to exhibit high carrier mobility, good conductivity, and stable adaptability, which are urgently required for use in various state-of-art microelectronic devices. Of these materials, intrinsic graphene has been theoretically predicted to possess extremely high carrier mobility, excellent thermal conductivity, high visible light transmittance, and high mechanical strength, and thus, has attractive potential functional applications. However, it is difficult to maintain these excellent properties in applications because they are sensitive to the interfacial contact of graphene with other components in the devices [4]. Many approaches have been reported to modify the properties of graphene, such as by decorating the edges of graphene [5], introducing dopant atoms in graphene [6], and choosing a suitable supporter [7]. Previous investigations have indicated that the performances of graphene and those of whole graphene/supporter stacked structures are dominantly influenced by the supporting underlayer [8–12]. The wide bandgap of h-BN and its low lattice mismatch (1.8%) with graphene render it attractive for use as a dielectric supporter for graphene [13]. Graphene on h-BN (G/h-BN) exhibits its own unique electrical properties, which creates wide prospects for its application in the fabrication of nanoelectronic

devices [14–16]. Furthermore, the deep ultraviolet absorption and excellent mechanical, thermal, and chemical stability of BN make the G/h-BN stacked structure promising for use in optical and thermal devices, UV detectors, electron field emission and electrochemical detection [17–24].

Currently, the assembly of G/h-BN structure is a complicated multistep process. After the separate mechanical exfoliation of both h-BN and graphene films, the h-BN and graphene should be carefully transferred onto the supporter, in sequence [25–27]. However, the scaling up of this exfoliation and transfer process for large-scale fabrication is difficult. Moreover, the precursors used in the conventional chemical vapour deposition (CVD) method to synthesize h-BN are poisonous and explosive [28]. In this paper, we propose a different approach to fabricate G/h-BN stacked structures, without any exfoliation or transfer processes. The underlayer h-BN film was deposited via sputtering, and it was used as a catalyst for the growth of graphene in the subsequent chemical vapour deposition process. Fabrication parameters, such as deposition time and RF power of the SiO_2/Si substrate during sputtering, as well as the temperature and cooling-down speed during low pressure chemical vapour deposition (LPCVD), were optimized, and it proved to be crucial to the growth of graphene. The mechanism of graphene growth and the effect of BN as the catalyst are also discussed in this paper.

2. EXPERIMENTAL DETAILS

h-BN films were first deposited under Ar and N_2 atmosphere using an RF-magnetron sputtering system (FJL560C3, Shenyang Scientific Instruments Research Institute, China) on a Si (100) substrate with a 300 nm thick SiO_2 layer. The image of the substrate surface in an atomic force microscope (AFM, Nano IR 2-fs, BRUKER, USA) was provided in Fig. 1 with the surface height inserted. The average roughness (R_a) of the substrate surface was measured to be 0.15 nm. The size of the substrate is 20 mm × 20 mm, which is small enough to ensure to obtain the same thickness of a boron nitride film in the centre and at the periphery of the substrate during the sputtering process. The h-BN target (99.99% purity) of 60 mm diameter and 5 mm thickness was purchased from Beijing CHINO New Materials Co., Ltd., China. The substrate was kept at 500°C during the sputtering process. The sputtering pressure was 0.5 Pa. Subsequent to sputtering the samples were annealed in a high-temperature tube furnace (T1780A, Henan Chengyi Laboratory Equipment Co., Ltd., China) to enhance the crystallinity of the BN films. The annealing temperature and holding time were 1000°C and 120 min, respectively. CH_4 and H_2 were used in the ratio of 50:5 to synthesize graphene and the total pressure was kept to 80 Pa during the

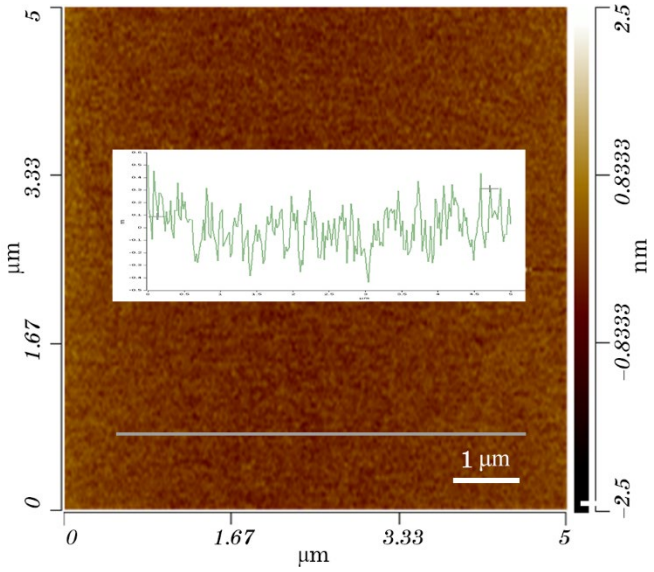

Fig. 1. AFM image of the SiO_2/Si substrate.

whole period. Finally, graphene was directly deposited on the h-BN films when the mixed gases were heated under different temperatures and held for a period of time, without any metal catalyst, in a low-pressure chemical vapour deposition system (LPCVD, Lindberg/Blue M, Thermo Fisher Scientific, USA) to form G/h-BN stacked films. The surface morphology of the films was characterized by atomic force microscopy (AFM, Dimension Icon–, BRUKER, USA), and the experimental data were analysed by NanoScope Analysis software. The elemental distribution on the film surface was analysed via x-ray photoelectron spectroscopy (XPS, ESCALAB 250, Thermo Fisher Scientific, USA). The films were also characterized using a Raman microscope (inVia, Renishaw, UK).

3. RESULTS AND DISCUSSION

3.1. Characterization of h-BN and G/h-BN Films

An optimal surface roughness of the sputtered h-BN films is important for obtaining high quality graphene during CVD. Figure 2, *a*, *b* are the AFM images of an h-BN film after annealing and after depositing graphene, respectively. The average surface roughness of the sample shown in Fig. 2, *a* was 0.364 nm, which proves that the surface of the BN film was flat except for some large particles that were formed during annealing. Several holes were present on the surface of the film af-

ter graphene deposition (Fig. 2, *b*) and its average surface roughness has increased to 16.3 nm. The variations in the surface height of the BN film and G/h-BN can be seen from the insets in Fig. 2, *a*, *b*, respectively. Figure 2, *c* is the SEM image of the G/h-N film. Several particles and holes could be seen in this image and in coordination with the result of AFM.

The Raman spectrum of the G/h-BN film is shown in Fig. 3. The intensity of the D peak (I_D) was high and a weak shoulder peak, D′, appeared to the right side of the G peak, which indicates that there were some defects in the graphene. The value of half width of the 2D peak was 62.5 cm^{-1}, which indicates that the crystallization degree of graphene was not high enough. The ratio of I_D/I_G and I_{2D}/I_G were 0.40 and 0.70, respectively, where I_D, I_G, and I_{2D} are the intensities of peaks D, G, and 2D, respectively. Raman mapping of G/h-BN (Fig. 4) shows that the intensities of the D and G peaks were relatively uniform,

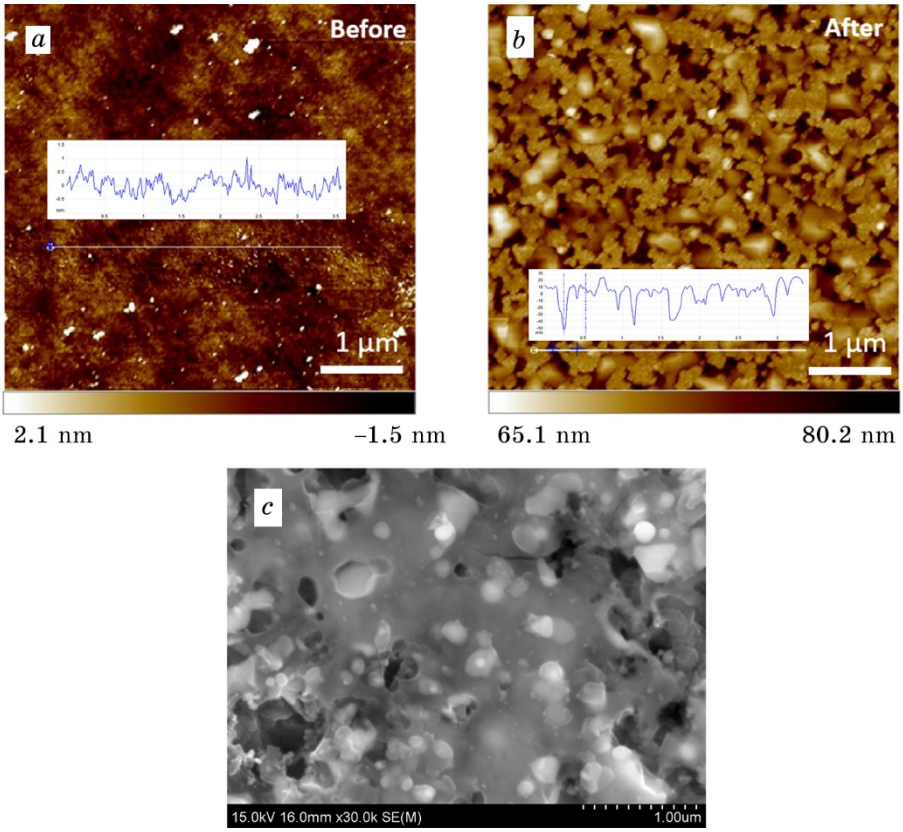

Fig. 2. AFM image of h-BN film (*a*), AFM image (*b*) and SEM image (*c*) of the G/h-BN stacked film.

which indicates that the distribution of graphene defects and the degree of graphitization were very uniform in the whole mapping test range. The intensity variation of 2D peak was related to the flatness degree of the BN film and the thickness of graphene at the test position. Figure 4, *d* shows the Raman spectral image of the I_{2D}/I_G intensity ratio of graphene. The ratio varied from 0.446 to 1.223, which can be attributed to the variation of graphene layers and the stretching of graphene caused by the different flatness of the BN film [29].

The chemical bonding information of the G/h-BN film was obtained via XPS analysis, and the results are shown in Fig. 5. In Figure 5, *a*, the characteristic peak of B is not obvious and the signal to noise ratio is low. This peak was fitted into two peaks. The fitted peak at 191.1 eV was close to the binding energy of B (191.0 eV) in h-BN. A small shoulder at a lower binding energy of 189.5 eV is considered to be the contribution from the bonding configuration of B and C, since C atoms have a lower electronegativity than N.

The intensity of the characteristic peak of C is high (Fig. 5, *b*). After fitting and splitting, the original curve was fitted into three peaks as shown in red. Of these three peaks, the middle one is located at 284.6 eV, which is close to the binding energy of the C–C bond. The left shoulder located at 283.5 eV is due to the B–C bond, and the right shoulder located at 285.7 eV is due to the N–C bond. Figure 5, *c* shows the characteristic peak of N. The peak, located at 398.3 eV, was close to the binding energy of B–N (398.2 eV). The left shoulder located at 396.7 eV may be due to the N–Si bond which arises due to the binding

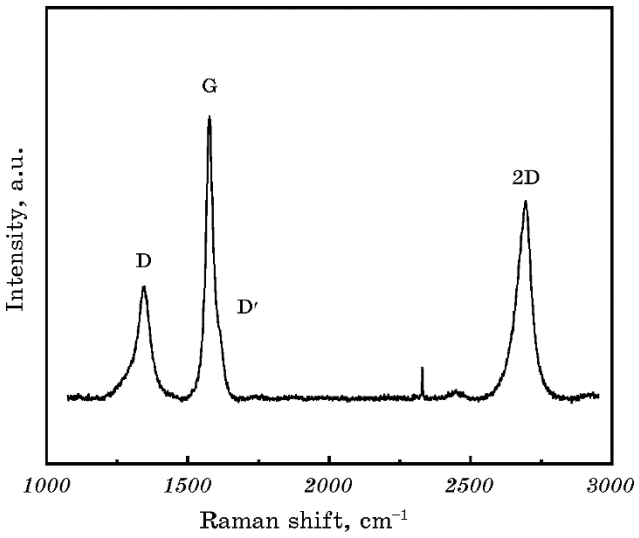

Fig. 3. Raman spectrum of G/h-BN.

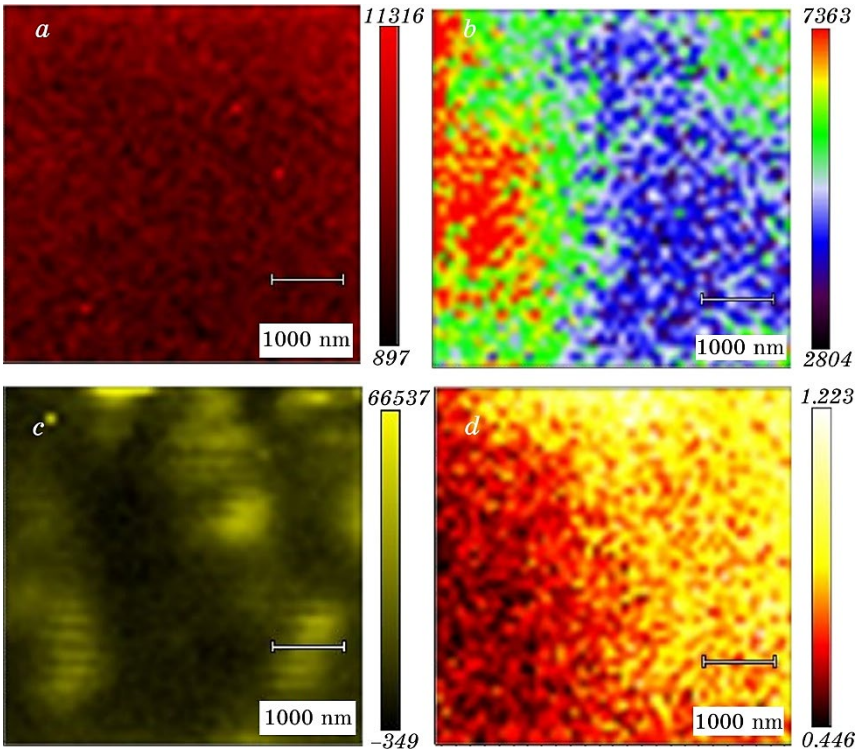

Fig. 4. Raman mapping of G/BN at D peak (*a*), G peak (*b*), 2D peak (*c*), and I_{2D}/I_G value (*d*).

of N atoms to the Si substrate. The right shoulder located at 398.9 eV is due to the C–N bond. The atomic percentages of C, B, and N in the G/h-BN film are 96.07%, 2.39%, and 1.54%, respectively. The average sheet resistivity was 3750 $\Omega \cdot sq^{-1}$ which is much larger than that of pure graphene. The B–C bond and N–C bond caused by B and N co-doping might have a great influence on the electrical property of the G/h-BN composite film.

3.2. Effect of Deposition Temperature and Time

The quality of G/h-BN film under different deposition temperatures was investigated *via* Raman spectroscopy (Fig. 6). The Raman spectral analysis data of G/h-BN films at different deposition temperatures is provided in Table 1. As can be seen from Fig. 6, when the deposition temperature is 800°C, there is no Raman signal corresponding to graphene. The peaks located at 1305 cm^{-1} and 1366 cm^{-1} is from different boron nitride phases. This is because CH_4 rarely pyrolyses at 800°C; furthermore, it is very difficult for carbon atoms to be deposited on the

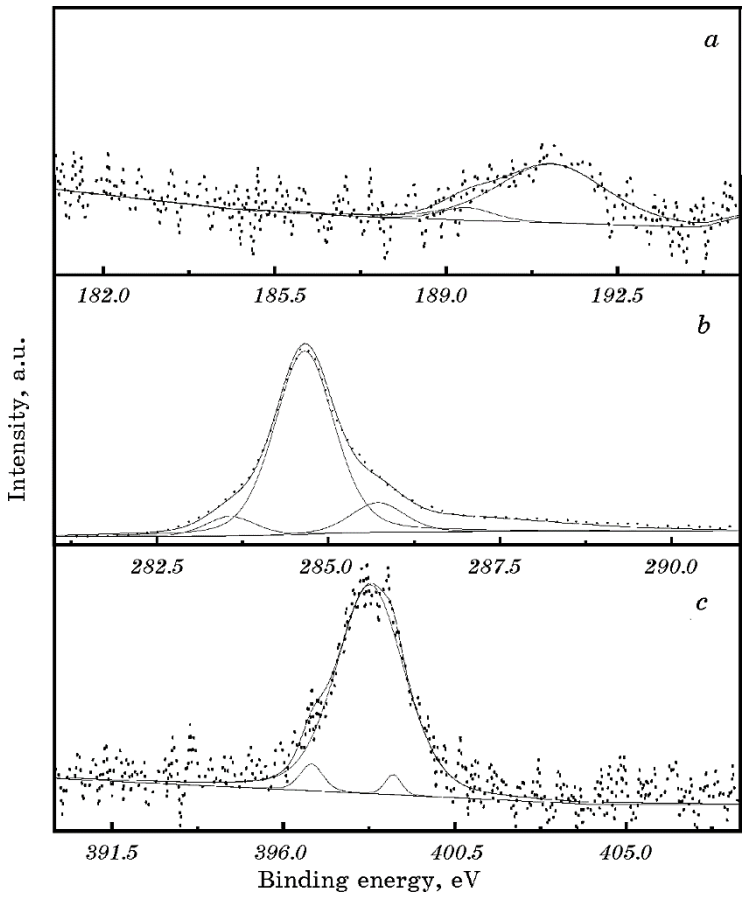

Fig. 5. XPS spectra characteristic of B (*a*), C (*b*), and N (*c*) on G/h-BN film surface.

substrate as most of the CH_4 was pumped out. When the temperature was increased further to 900°C, graphene was deposited on the substrate.

The value of I_{2D}/I_G is 1.22 when graphene is deposited at 900°C (Table 1), indicating that a few layers of graphene was formed. However, the D peak is very high and the value of I_D/I_G is nearly equal to 1.75, which implies that the as-prepared graphene has some defects. In addition, a shoulder peak, D′, is observed to the right of the G peak, further proving the existence of the defects in graphene. When the temperature was increased further to 1000°C, I_{2D}/I_G was approximately 1.07, and I_D/I_G was 0.84. The D′ peak on the right shoulder of the G peak is less obvious for this sample compared with that of graphene deposited at 900°C. The above results indicate that the quality of graphene is im-

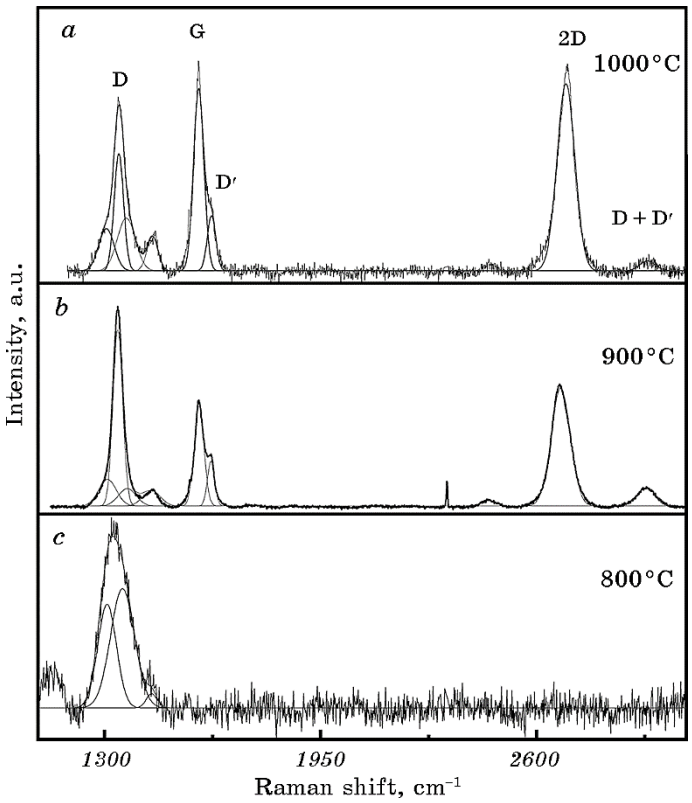

Fig. 6. Raman spectra of G/h-BN fabricated at different deposition temperature: 1000°C (*a*); 900°C (*b*); 800°C (*c*), all deposition time was 120 min.

proved when the deposition temperature is increased from 900°C to 1000°C.

In the process of CVD, deposition time is also an important parameter that significantly affects the quality of graphene. Figure 7, *c* shows that when the deposition time is 30 min, there is no Raman signal characteristic of graphene. This is because 30 min is too short for the carbon atoms to be deposited on the substrate and to form a continuous graphene film. When the deposition time was increased from 30 to 60 min, the characteristic peaks of graphene are obvious. The values of $I_D/I_{D'}$, I_D/I_G, and I_{2D}/I_G are listed in the Table 2. There is only a slight difference in the value of I_{2D}/I_G with change in the deposition time from 60 to 120 min. However, when the deposition time is 120 min, the value of I_D/I_G is significantly higher than that of graphene deposited for 60 min. Therefore, it can be concluded that the number of graphene layers remains unchanged, but the defects of graphene increase considerably when the deposition time is prolonged. In Figure 7, *a*, the

TABLE 1. Raman spectral analysis data of G/h-BN films fabricated at different deposition temperatures.

Deposition temperature (°C)	I_D/I_D'	I_D/I_G	I_{2D}/I_G
1000	1.23	0.84	1.07
900	3.87	1.75	1.22
800	–	–	–

peak at about 1300 cm^{-1} is superposed by a cubic BN phase peak (peak A, located at 1305 cm^{-1}), hexagonal BN phase peak (peak C, located at 1366 cm^{-1}), and D peak of graphene (peak B, located at 1340 cm^{-1}). When the growth time is 60 min, the D′ peak appears to the right side of the G peak (Fig. 7, *b*), indicating that there are still a lot of defects in the graphene film. In Figure 7, *a*, there is no obvious shoulder to the right side of the G peak, which indicates that the type of defects in the graphene deposited for 120 and 60 min might be different.

3.3. Investigation of the Deposition Mechanism of Graphene

To investigate the deposition mechanism of graphene, we prepared the G/h-BN films at different cooling rates on h-BN substrates. It was observed that graphene was deposited on all substrates at a slow cooling rate of approximately 20°C/min, and the specimens cooled within the furnace. However, when cooling at a faster rate, *i.e.*, the quartz tube holding specimens was brought out of the furnace and cooled in air, the characteristic peaks of graphene were not evident in the Raman spectra. This indicates that the growth mechanism of the deposited graphene on the h-BN substrate is epitaxial growth, as previously reported [30, 31]. The deposition of graphene on h-BN is not simply the ac-

TABLE 2. Raman spectral analysis data of G/h-BN films fabricated under different deposition times.

Deposition time (min)	I_D/I_D'	I_D/I_G	I_{2D}/I_G
120	–	2.04	1.21
60	2.35	0.66	0.86
30	–	–	–

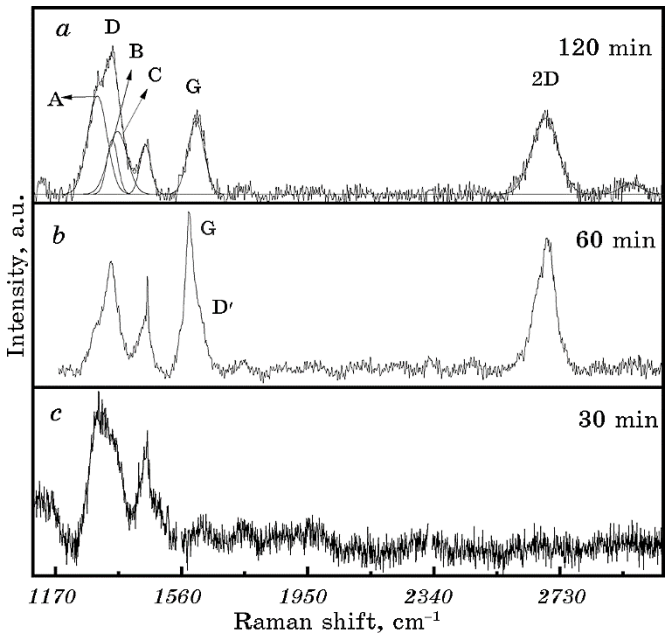

Fig. 7. Raman spectra of G/h-BN fabricated under different deposition times: 120 min (*a*); 60 min (*b*); 30 min (*c*), all deposition temperature was 1000°C.

cumulation of carbon atoms on the substrate surface; the slow cooling rate is important for carbon atoms to have enough time to grow along the crystal growth direction of h-BN. Therefore, it is necessary to explore the impact of the h-BN substrate on the growth of graphene of different film thicknesses by varying the sputtering time.

Figure 8 depicts the Raman spectra of graphene films deposited on h-BN fabricated under different sputtering durations. The wide peak on the left can be fitted into three peaks of cubic boron nitride, hexagonal boron nitrogen and the D peak of graphene (Fig. 8, *d*). The shoulder D′ located to the right of the graphene G peak appears for all the samples prepared at different sputtering durations. However, the shoulder was significantly shorter for the sample with the h-BN fabricated with 30 min of sputtering time.

We analysed the peaks in Fig. 8 and summarized the data in Table 3. The I_D/I_G ratio of graphene deposited on the h-BN substrate which the thickness was 32 nm reached the highest value 1.62. When the h-BN thickness reached 280 nm, the I_D/I_G decreased to 0.85 and I_{2D}/I_G ratio exceeded 1, indicating the high-quality graphene has formed. It can be presumed that with the increase of the h-BN film thickness, the size of the synthesized graphene regions increases and therefore the role of edge effects in such regions decreases. That is, the structural defects

caused by unclosed aromatic rings of graphene decreased when the h-BN film turned thicker with less defects.

Furthermore, we deposited graphene on h-BN prepared using different sputtering powers. With an increase in the sputtering power, the full width at half maximum (FWHM) of the Raman characteristic 2D peak increased gradually (Fig. 9), indicating that the crystallinity of graphene decreased gradually. As can be seen from Table 4, this FWHM increases with an increase in the sputtering power, indicating that the crystallinity of graphene decreases by increasing the sputtering power of BN. Furthermore, the gradual decrease in I_{2D}/I_G indicates that the number of graphene layers increased with the increase in sput-

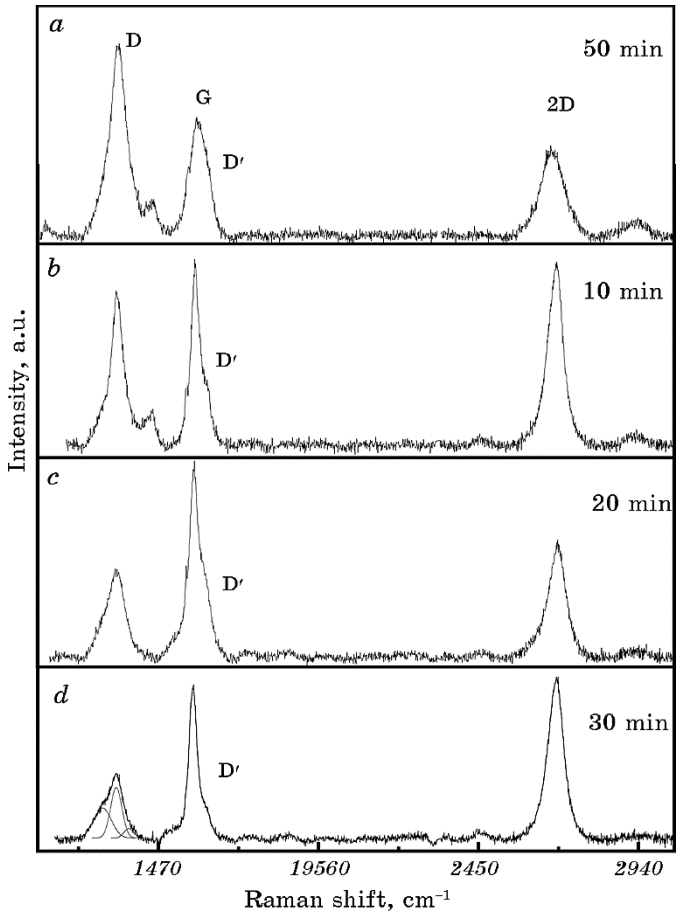

Fig. 8. Raman spectra of G/h-BN fabricated under different BN sputtering times: 5 min (*a*); 10 min (*b*); 20 min (*c*); 30 min (*d*), all deposition temperature and time of graphene were 1000°C and 120 min, respectively, and BN sputtering power was 80 W.

TABLE 3. Raman spectral analysis data of graphene on h-BN films fabricated under different sputtering times.

Sputtering time (min)	Film thickness (nm)	I_D/I_G	I_{2D}/I_G
30	280	0.85	1.01
20	150	0.79	0.85
10	72	0.92	0.99
5	32	1.62	0.73

TABLE 4. Raman spectral analysis data of graphene on h-BN films fabricated under different BN sputtering power.

Sputtering power (W)	FWHM (cm^{-1})	I_D/I_G	I_{2D}/I_G
150	103	0.81	0.34
100	68	0.41	0.71
80	61	0.91	0.99

tering power. When the sputtering power is 100 W, the I_D/I_G value is minimum, indicating the presence of the least number of defects.

4. CONCLUSIONS AND PROSPECT

G/h-BN stacked films were successfully synthesized by RF-magnetron sputtering and subsequent LPCVD. The parameters of deposition time and RF power during sputtering were optimized to fabricate h-BN, which also functioned as a catalyst for the epitaxial growth of graphene. Furthermore, a high deposition temperature, long deposition time and low cooling-down speed were proved to be necessary to facilitate the growth of graphene. The h-BN film with low roughness and high thickness was experimentally verified to be an effective alternative to metal catalysts in the CVD of graphene. The B–C bond and N–C bond caused by B and N co-doping have been found in the G/h-BN composite film, and the existence of these bonds makes it possible for this composite to be applied in the field of physics one day when the perfect single- or double-layer graphene synthesized through this proposed technology. The influence of the morphology, structure and crystallin-

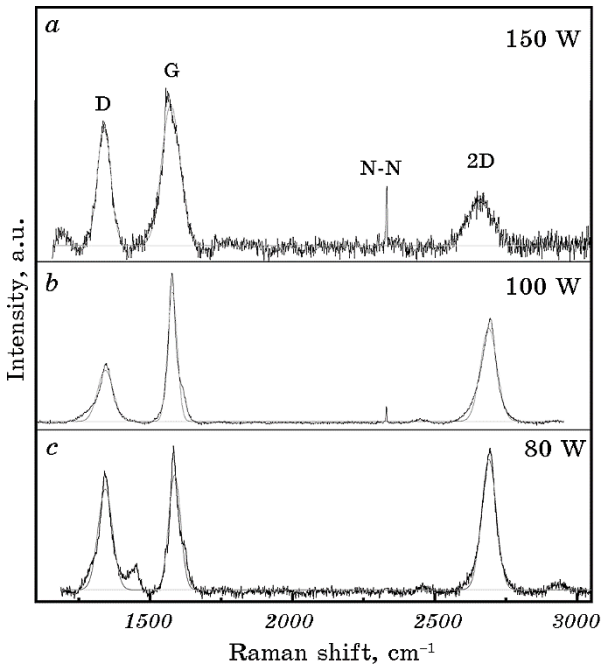

Fig. 9. Raman spectra of graphene film under different value of BN sputtering power: 150 W (*a*); 100 W (*b*); 80 W (*c*), all deposition temperature and time of graphene were 1000°C and 120 min, respectively, and BN sputtering time was 10 min.

ity of BN film on the deposition of graphene is also worthy to be investigated in future.

ACKNOWLEDGEMENT

This contribution was created under the support of projects High-level Talents' Discipline Construction Fund of Shandong University (31370089963078) and Shandong Provincial Science and Technology Major Project(2019GGX101029).

REFERENCES

1. A. K. Geim and K. S. Novoselov, *Nat. Mater.*, 6: 183 (2007).
2. M. Bokdam, P. A. Khomyakov, G. Brocks, Z. Zhong, and P. J. Kelly, *Nano Lett.*, **11**: 4631 (2011).
3. K. F. Mak, K. He, C. Lee, G. H. Lee, J. Hone, T. F. Heinz, and J. Shan, *Nat. Mater.*, **12**: 207 (2013).
4. D. R. Cooper, B. D'Anjou, N. Ghattamaneni, B. Harack, M. Hilke, A. Horth,

N. Majlis, M. Massicotte, L. Vandsburger, E. Whiteway, and V. Yu, *Int. Sch. Res. Notw. ISRN Condens. Matter Phys.*, 2012: 501686 (2012).
5. O. Hod, V. Barone, J. E. Peralta, and G. E. Scuseria, *Nano Lett.*, **7**: 2295 (2007).
6. L. Ci, L. Song, C. Jin, D. Jariwala, D. Wu, Y. Li, A. Srivastava, Z. F. Wang, K. Storr, L. Balicas, F. Liu, and P. M. Ajayan, *Nat. Mater.*, **9**: 430 (2010).
7. M. Son, H. Lim, M. Hong, and H. C. Choi, *Nanoscale*, **3**: 3089 (2011).
8. S. Fratini and F. Guinea, *Phys. Rev. B*, **77**: 195415 (2008).
9. T. Ando, *J. Phys. Soc. Jpn.*, **75**: 074716 (2006).
10. J. H. Chen, C. Jang, S. Xiao, M. Ishigami, and M. S. Fuhrer, *Nat. Nanotechnol.*, **3**: 206 (2008).
11. J. Yan and M. S. Fuhrer, *Phys. Rev. Lett.*, **107**: 206601 (2011).
12. L. Liao, J. Bai, Y. Qu, Y. Huang, and X. Duan, *Nanotechnology*, **21**: 015705 (2009).
13. G. Giovannetti, P. A. Khomyakov, G. Brocks, P. J. Kelly, and J. van den Brink, *Phys. Rev. B*, **76**: 073103 (2007).
14. C. R. Dean, A. F. Young, I. Meric, C. Lee, L. Wang, S. Sorgenfrei, K. Watanabe, T. Taniguchi, P. Kim, K. L. Shepard, and J. Hone, *Nat. Nanotechnol.*, **5**: 722 (2010).
15. P. Sutter, J. Lahiri, P. Zahl, B. Wang, and E. Sutter, *Nano Lett.*, **13**: 276 (2013).
16. J. Wang, F. Ma, W. Liang, and M. Sun, *Mater. Today Phys.*, **2**: 6 (2017).
17. V. Mughnetsyan, *Superlattices Microstruct.*, **147**: 106700 (2020).
18. T. Ouyang, Y. Chen, Y. Xie, K. Yang, Z. Bao, and J. Zhong, *Nanotechnology*, **21**: 245701 (2010).
19. Y. Kubota, K. Watanabe, O. Tsuda, and T. Taniguchi, *Science*, **317**: 932 (2007).
20. R. Jerome and A.K. Sundramoorthy, *Anal. Chim. Acta*, **1132**: 110 (2020).
21. X. D. Hong, H. R. Zheng, and D. Liang, *Mater. Lett.*, **277**: 128356 (2020).
22. S. D. Nehate, A. K. Saikumar, A. Prakash, and K. B. Sundaram, *Mater. Today Adv.*, **8**: 100106 (2020).
23. K. Zhour, F. E. H. Hassan, H. Fahs, and M. Vaezzadeh, *Mater. Today Commun.*, **21**: 100676 (2019).
24. Z. Dai, F. Wen, and Z. Yang, *Mater. Lett.*, **232**: 58 (2018).
25. T. Taniguchi and K. Watanabe, *J. Cryst. Growth*, **2**: 525 (2007).
26. Z. Liu, L. Song, S. Zhao, J. Huang, L. Ma, J. Zhang, J. Lou, and P. M. Ajayan, *Nano Lett.*, **11**: 2032 (2011).
27. M. Wang, S. K. Jang, W.-J. Jang, M. Kim, S.-Y. Park, S.-W. Kim, S.-J. Kahng, J.-Y Choi, R. S. Ruoff, Y. J. Song, and S. Lee, *Adv. Mater.*, **25**: 2746 (2013).
28. H. Wang, X. Zhang, J. Meng, Z. Yin, X. Liu, Y. Zhao, and L. Zhang, *Small*, **11**: 1542 (2015).
29. K. M. Hu, Z. Y. Xue, Y. Q. Liu, H. Long, B. Peng, H. Yan, Z. F. Di, X. Wang, L. W. Lin, and W. M. Zhang, *Small*, **15**: 1804337 (2019).
30. W. Yang, G. Chen, Z. Shi, C.-C. Liu, L. Zhang, G. Xie, M. Cheng, D. Wang, R. Yang, D. Shi, K. Watanabe, T. Taniguchi, Y. Yao, Y. Zhang, and G. Zhang, *Nat. Mater.*, **12**: 792 (2013).
31. T. Gao, X. Song, H. Du, Y. Nie, Y. Chen, Q. Ji, J. Sun, Y. Yang, Y. Zhang, and Z. Liu, *Nat. Commun.*, **6**: 6835 (2015).